Near-infrared fluorescent proteins for multicolor *in vivo* imaging

Daria M Shcherbakova[1,2] & Vladislav V Verkhusha[1,2]

Near-infrared fluorescent proteins (FPs) are in high demand for *in vivo* imaging. We developed four spectrally distinct near-infrared FPs—iRFP670, iRFP682, iRFP702 and iRFP720—from bacterial phytochromes. iRFPs exhibit high brightness in mammalian cells and tissues and are suitable for long-term studies. iRFP670 and iRFP720 enable two-color imaging with standard approaches in living cells and mice. The four new iRFPs and the previously engineered iRFP713 allow multicolor imaging with spectral unmixing in living mice.

Deep optical imaging in mammalian tissues and whole mammals requires near-infrared (NIR) fluorescent probes. In the so-called NIR 'optical window' (from 650 nm to 900 nm), mammalian tissue is more transparent to light because the combined absorption of hemoglobin, melanin and water is minimal[1]. In addition, reduced autofluorescence and low light scattering make this spectral region preferable for deep-tissue imaging.

Efforts to engineer GFP-like FPs into far-red probes have resulted in several FPs shown to be useful in mammals, such as E2-Crimson[2], mNeptune[3], TagRFP657 (ref. 4), eqFP650 (ref. 5) and eqFP670 (ref. 5). Among these, TagRFP657 exhibits the most red-shifted excitation maximum at 611 nm but suffers from low brightness. The photoconverted form of the photoswitchable PSmOrange[6] has an excitation peak at 634 nm; but to appear, this form requires photoconversion of the FP with blue light, which penetrates mammalian tissues poorly.

Bacterial phytochrome photoreceptors (BphPs) are promising templates for the engineering of NIR FPs[7]. Phytochromes, which are found in plants, fungi, bacteria and cyanobacteria, are a superfamily of photoreceptors that use different types of tetrapyrroles as chromophores. Members of the BphP subfamily are the most attractive source for FP development because they have the most red-shifted absorption spectra among the phytochromes and because they use the chromophore biliverdin IVα (BV), which is an intermediate of heme metabolism and is ubiquitous in mammalian tissues[8,9]. Wild-type BphPs exhibit multidomain architecture, which typically consists of the PAS, GAF, PHY and effector domains. BphPs generally adopt two spectrally different photochemical states—red absorbing (Pr) and either far-red absorbing (Pfr) or, more rarely, near-red absorbing (Pnr)[10]. Absorption maxima vary by BphP and photochemical state[8]. Deletion of the PHY and effector domains from the BphPs of *Deinococcus radiodurans* (*Dr*BphP) and *Rhodopseudomonas palustris* (*Rp*BphP2) followed by extensive mutagenesis of the PAS and GAF domains resulted in the generation of several NIR FPs: IFP1.4 (excitation/emission maxima at 684 nm/708 nm)[11], Wi-Phy (701 nm/719 nm)[12] and iRFP (692 nm/713 nm)[13]. IFP1.4 and iRFP were previously used for whole-body imaging[11,13,14]. IFP1.4 required injection of BV to become fluorescent, but iRFP efficiently incorporated endogenous BV, making iRFP as easy to use as conventional GFP-like FPs[13]. iRFP was applied for live imaging of livers[13] and tumors[14] in mice.

Having several spectrally distinct NIR FPs could open new possibilities for labeling two or more tissues or organs and for tracking several cell populations in a live animal. Here we report four NIR FPs derived from BphPs, termed iRFP670, iRFP682, iRFP702 and iRFP720 after the maxima of their emission peaks. To avoid confusion, we refer to the original iRFP as iRFP713. A palette of iRFPs enables multicolor NIR imaging *in vivo*.

We started from *Rp*BphP6 (ref. 8) as a template for further NIR FP engineering. *Rp*BphP6 has an absorbance maximum in the Pr state at 700 nm, 10 nm shorter than the maximum for *Rp*BphP2 (the template for the derivation of iRFP713). First, we cut *Rp*BphP6 to only the PAS and GAF domains, which are required to covalently incorporate BV[15]. Mutations of the invariant key residue Asp202 and the substitution Y258F (numbering follows that for *Rp*BphP2) were shown to stabilize the chromophore in the Pr state and render the protein fluorescent[12,16] (**Supplementary Fig. 1**). We performed saturated mutagenesis of the Asp202 and adjacent Ile203 positions. The brightest mutants had the substitution combination of either D202V and I203V or D202L and I203V. After three rounds of random mutagenesis, we tested the best mutants for brightness in transiently transfected HeLa cells to eliminate proteins with poor efficiency of folding and poor incorporation of BV[13]. A final variant, iRFP702, had excitation and emission maxima at 673 nm and 702 nm, respectively.

We then searched for spectrally shifted variants of iRFP713 and iRFP702 by randomly mutating them and screening the mutants using FACS, collecting mutants with blue- and red-shifted spectra in each library. Additionally, we targeted key protein positions 180, 202, 203 and 254 using saturated mutagenesis. After testing spectral properties and effective brightness in HeLa cells, we chose three final variants: iRFP670 (excitation/emission maxima at 643 nm/670 nm), iRFP682 (663 nm/682 nm) and iRFP720 (702 nm/720 nm) (**Table 1** and **Fig. 1a,b**). Absorbance spectra (**Fig. 1c**) indicated that all iRFPs efficiently incorporated the BV chromophore, as the side peaks at 280 nm and 390 nm (corresponding to the absorbance of BV) are substantially smaller than the main peaks[13].

[1]Department of Anatomy and Structural Biology, Albert Einstein College of Medicine, Bronx, New York, USA. [2]Gruss-Lipper Biophotonics Center, Albert Einstein College of Medicine, Bronx, New York, USA. Correspondence should be addressed to V.V.V. (vladislav.verkhusha@einstein.yu.edu).

RECEIVED 21 FEBRUARY; ACCEPTED 22 MAY; PUBLISHED ONLINE 16 JUNE 2013; DOI:10.1038/NMETH.2521

Table 1 | Properties of BphP-derived NIR FPs used for *in vivo* imaging

NIR FP	BphP template	Ex. (nm)	Em. (nm)	Extinction coefficient (M^{-1} cm^{-1})	Quantum yield (%)	Molecular brightness vs. iRFP (%)	Photostability, $t_{1/2}$ (s)	pK_a	Brightness in HeLa cells vs. iRFP (%)
IFP1.4	*Dr*BphP	684	708	102,000	7.0	116	70	4.6	8
iRFP670	*Rp*BphP6	643	670	114,000	11.1	205	290	4.0	119
iRFP682	*Rp*BphP2	663	682	90,000	11.3	165	490	4.5	105
iRFP702	*Rp*BphP6	673	702	93,000	8.2	124	630	4.5	61
iRFP713 (formerly iRFP)	*Rp*BphP2	690	713	98,000	6.3	100	960	4.5	100
iRFP720	*Rp*BphP2	702	720	96,000	6.0	93	490	4.5	110

Ex., excitation peak; Em., emission peak; $t_{1/2}$, photobleaching half time.

Thus, the molecular evolution of RpBphP6-PAS-GAF and iRFP713 resulted in four new NIR FPs with absorbance and fluorescence maxima covering ~50 nm of the respective NIR ranges (**Fig. 1d**).

The molecular brightness (the product of a molar extinction coefficient and quantum yield) of the new iRFP variants was similar to the brightness of iRFP713 and IFP1.4 (**Table 1**). Like the templates they are based on[11,15], the new iRFPs are dimeric and do not contain monomerizing mutations at the C termini of their GAF domains[11,12]. The fluorescence of all iRFPs was stable at pH values between 4 and 8, with pK_a values of 4.0 for iRFP670 and 4.5 for other iRFPs (**Supplementary Fig. 2a**). To compare folding and chromophore incorporation kinetics of BphP-based FPs with those of conventional GFP-like FPs, we monitored fluorescence in bacteria upon pulse-chase induction of protein expression. All BphP-based FPs had half times (that is, time to reach half of the maximum fluorescence) for combined folding and chromophore formation comparable to that of EGFP: 4.5–5 h for iRFPs and IFP1.4 compared to 3 h for EGFP (**Supplementary Fig. 2b**).

High effective brightness in mammalian cells without addition of exogenous BV is a key advantage of iRFP713 over IFP1.4. We analyzed the effective brightness of the newly developed iRFPs in transiently transfected HeLa cells. No external BV was added. The highest fluorescence signal was obtained for iRFP670 (119% of that for iRFP713); the lowest, for iRFP702 (61%) (**Fig. 1e**). The effective brightness—which depends on molecular brightness, intracellular stability, affinity for BV and protein expression level—reveals that the new iRFPs could be as efficient imaging tools as iRFP713.

Epifluorescence microscopy of HeLa cells revealed evenly distributed fluorescence for all iRFPs (**Supplementary Fig. 3a**). The intracellular photostability of the four iRFPs was lower than that of iRFP713 but higher than that of IFP1.4 (**Table 1** and **Supplementary Fig. 3b**).

We also compared the fluorescence signal of transiently transfected HeLa cells expressing iRFP670 to the signal of cells expressing the GFP-like far-red FPs E2-Crimson, mNeptune, eqFP650 and eqFP670 (**Supplementary Fig. 4**). iRFP670 had mean fluorescence intensities sixfold higher than the intensities of these FPs, making it a promising variant for whole-cell labeling in applications involving standard red lasers.

To quantitatively compare the performance of iRFPs with that of other far-red FPs for deep-tissue imaging, we used a 'phantom' model engineered to have autofluorescence and light-scattering properties matching those of mouse muscle tissue. Equal amounts of purified FPs were placed inside the phantom at two depths (7.0 mm and 18.1 mm) and imaged in different spectral channels. We quantified the ratios of the fluorescence signal to autofluorescence background and compared the highest values for each FP among different filter channels (**Fig. 1f–i**). For the most blue-shifted iRFP670, the ratios were 5.6-fold higher at 7.0 mm and 11.7-fold higher at 18.1 mm than the ratios for mNeptune at these depths. For the most red-shifted iRFP720, the ratios were 9.5-fold higher at 7.0 mm and 18.9-fold higher at 18.1 mm than the respective ratios for mNeptune.

Fluorescence stability over cell generations indicates a lack of FP cytotoxicity and is critical for the application of FPs in living animals, especially in long-term studies[17]. To test for this, we compared iRFPs with the least cytotoxic standard, EGFP[2], in prolonged expression conditions. Preclonal mixtures of MTLn3 cells stably expressing FPs were analyzed by FACS 14 d after transfection and then 15 d after the first analysis (**Supplementary Fig. 5a**). Cells expressing the iRFPs retained more than half of the signal at the second time point, with the largest decrease of fluorescence (to 55%) observed in iRFP702-expressing cells and the smallest (to 84%) in iRFP682-expressing cells (**Supplementary Fig. 5b**); cells expressing EGFP retained 74% of their initial signal. A similar analysis with other mammalian cells resulted in 24% fluorescence retention for mKate2 and 73% fluorescence retention for E2-Crimson, the least cytotoxic far-red GFP-like FP[13].

To test the performance of iRFPs in whole-body imaging experiments, we used a mouse xenograft breast cancer model. MTLn3 cells stably expressing constructs for the different iRFPs were injected into the mammary glands of immunocompromised mice and grown into tumors. The high sensitivity of iRFPs as probes for *in vivo* imaging enabled detection of tumors at early stages (**Supplementary Fig. 5c**). We monitored the growth of the tumors by epifluorescence whole-body imaging for up to 4 weeks after cell injection (**Supplementary Fig. 6a**). Tumors expressing iRFPs produced high NIR fluorescence signal that constantly increased, in contrast to tumors expressing EGFP, whose signal increased only at the early stages (**Supplementary Fig. 6b**). The brightness of the tumors expressing each of the iRFPs correlated with the brightness levels of the different transgenic MTLn3 lines before injection (**Supplementary Fig. 6c**).

The 50-nm spectral shift between iRFP670 and iRFP720 should allow the use of these FPs in two-color imaging experiments. We quantified the fluorescence signals for each FP in two standard filter channels (excitation/emission maxima at 640 nm/680 nm and 710 nm/760 nm) (**Supplementary Fig. 7a**). The imaging contrast (calculated as the ratio between fluorescence signals of one FP and another FP in the two filter channels) was 690 for the iRFP670/iRFP720 pair and 510 for the iRFP670/iRFP713 pair.

We then used the iRFPs for two-color imaging in living mice. Two tumors expressing either iRFP670 or iRFP720 were implanted simultaneously into one mouse and grown close to each other, forming the conjoined tumor. The two spatially close fluorescent tissues could be distinguished using two filter channels

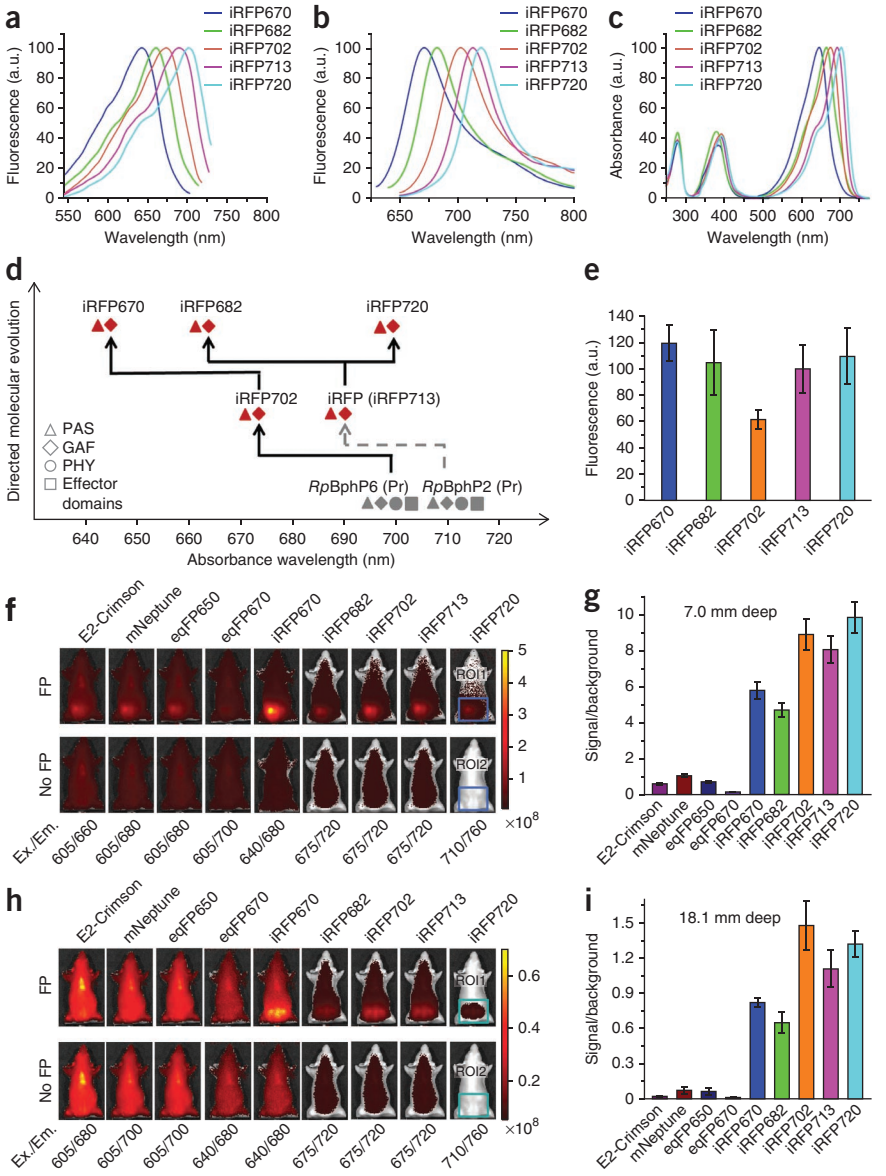

Figure 1 | Characterization of NIR FPs. (**a**,**b**) Normalized excitation (**a**) and emission (**b**) spectra of different iRFPs. (**c**) Normalized full absorbance spectra of iRFPs. (**d**) Schematic representation of directed molecular evolution that led to iRFPs with distinct spectral properties. The development of previously reported iRFP713 is shown with a dashed arrow. Pr, red-absorbing photochemical state. (**e**) Brightness of HeLa cells transiently transfected with iRFPs, normalized to the value for iRFP713-expressing cells. For each type of cell, the mean NIR fluorescence intensity of the cellular population was normalized to FP transfection efficiency (on the basis of cotransfected EGFP), excitation efficiency of each FP with the 635-nm laser, and fluorescence signal of each FP in the emission filter. Error bars, s.d. (n = 3 transfection experiments). (**f**) Comparison of iRFPs with GFP-like far-red FPs as fluorescent probes for deep-tissue imaging. Equal amounts of purified FPs (top row) or buffer with no FPs (bottom row) were imaged in epifluorescence mode inside a mouse phantom at 7.0-mm depth using several filter channels. Total radiant efficiencies of the indicated area with (ROI1) and without (ROI2) the FP sample were measured, and signal-to-background ratios ((ROI1 – ROI2)/ROI2) were calculated for each channel. Images with the highest ratio among channels are shown for each FP. The color bar indicates the total fluorescence radiant efficiency (photons s^{-1} cm^{-2} steradian^{-1} per μW cm^{-2}). (**g**) Quantification of the signal-to-background ratios for the images shown in **f**. (**h**,**i**) Comparisons as in **f**,**g** but with protein samples located 18.1 mm deep. Error bars, s.d.; n = 4 (**g**,**i**). a.u., arbitrary units; Ex., excitation maximum; Em., emission maximum.

(excitation/emission maxima at 640 nm/680 nm and 710 nm/760 nm) by whole-body imaging (**Fig. 2a**). The same was true for two tumors of unequal sizes implanted with a time difference of 1 week (**Supplementary Fig. 7b,c**).

Next we studied whether two different fluorescence sources could be spectrally separated inside an animal if they were located at different depths. Mice with a mammary gland tumor expressing iRFP670 were injected with iRFP713-encoding adenoviral particles that specifically infect mouse liver. As previously demonstrated[13], fluorescence in the liver was detected starting at the second day after infection. Liver expressing iRFP713 and the closely located tumor expressing iRFP670 could be spectrally separated (**Fig. 2b**). Using fluorescence imaging tomography, we could determine the localization of the two distinct fluorescent tissues in three dimensions (**Supplementary Fig. 8**). With *ex vivo* imaging of the isolated tumor and liver tissue, we confirmed iRFP670 and iRFP713 expression in these tissues (**Supplementary Fig. 9**).

To demonstrate that two-color NIR imaging is also possible with standard epifluorescence microscopy, we imaged HeLa cells expressing iRFP670 and either iRFP713 or iRFP720 in two different intracellular organelles: nucleus and mitochondria (**Fig. 2c** and **Supplementary Fig. 10**).

A potentially useful application of iRFPs would be the simultaneous detection of more than two types of cells, tissues or transcription activities with spectral imaging techniques. Four types of MTLn3 cells expressing iRFP670, iRFP682, iRFP702 or iRFP720 were detected as separate populations via flow cytometry (**Supplementary Fig. 11**) and via confocal microscopy with spectral detection (**Fig. 2d**). We next tested how many iRFPs we could spectrally 'unmix' *in vivo* using a standard whole-body imaging system with spectral detection, such as the IVIS Spectrum (PerkinElmer/Caliper). Using reference spectra for individual streaks, we distinguished five types of bacterial cells expressing iRFPs (**Supplementary Fig. 12**). In living mice, all five types of tumors also could be unmixed, starting as early as day 12 after the MTLn3 cell injection (**Fig. 2e**). We confirmed the specificity of the unmixing with *ex vivo* imaging of the isolated tumors (**Supplementary Fig. 13**).

Further studies revealing the chromophore photochemistry responsible for the spectral shifts in iRFPs should allow researchers to design new BphP-based probes with desired spectral properties. This in turn will open the door for the engineering of biosensors to noninvasively detect metabolites and enzymatic activities *in vivo*.

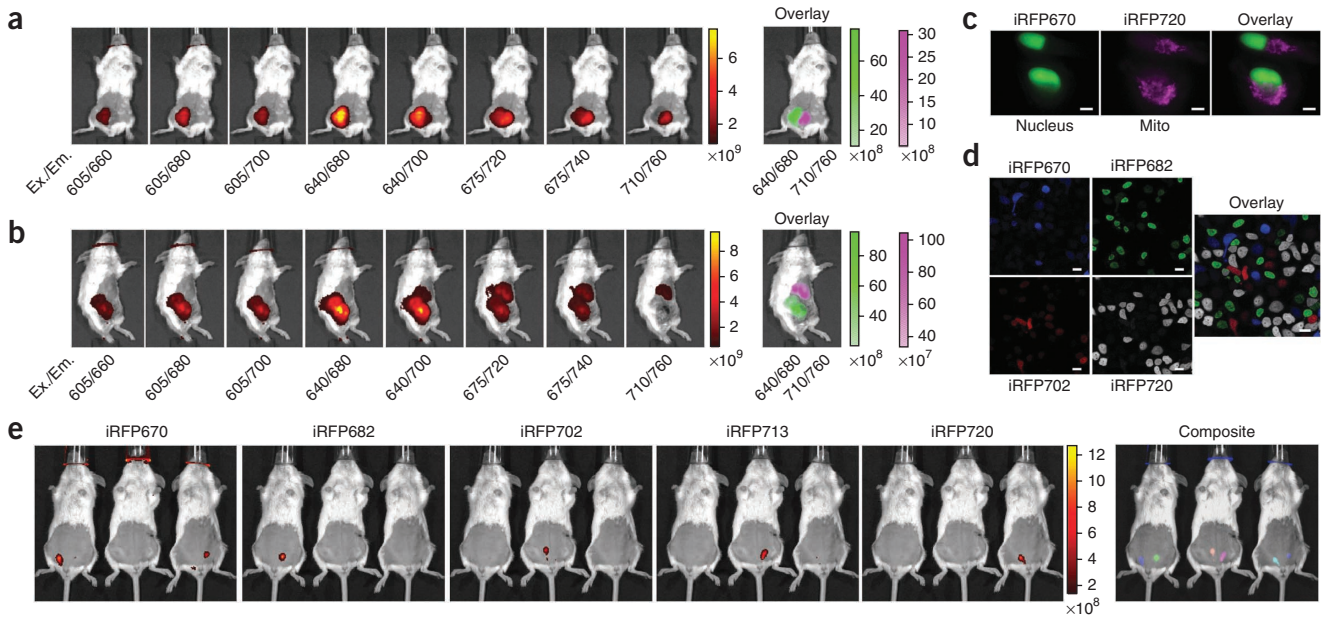

Figure 2 | Multicolor imaging *in vivo* and in cells. (**a**) Representative images of a living mouse with two injected tumors expressing iRFP670 (left tumor) and iRFP720 (right tumor). The images in different channels and the overlay of two optimal channels were obtained on day 24 after cell injections. (**b**) Representative images of a living mouse with a tumor expressing iRFP670 (lower left) and liver expressing iRFP713 (upper right). The images in different channels and the overlay of two optimal channels were obtained on day 29 after cell injection and day 6 after adenovirus infection. (**c**) Microscopy of HeLa cells coexpressing iRFP670 and iRFP720 in nucleus and mitochondria (Mito). Pseudocolor images (iRFP670 channel in green and iRFP720 channel in magenta) and the overlay are shown. Scale bars, 10 µm. (**d**) Confocal microscopy with spectral detection and linear unmixing of MTLn3 cells expressing iRFP670, iRFP682, iRFP702 and iRFP720. Emission was detected from 660 nm to 790 nm using excitation of a 633-nm laser. Unmixed channels and the overlay are shown in pseudocolors. Scale bars, 20 µm. (**e**) Separate detection of five types of tumors expressing iRFPs in living mice. Mice were injected with two types of MTLn3 cells each, from left to right in each image: iRFP670, iRFP682, iRFP702, iRFP713 and iRFP720. Images were acquired in 19 spectral channels on day 12 after cell injections and unmixed using reference spectra. Representative images of mice in unmixed channels and the composite pseudocolored image are shown. Color bars (**a**,**b**,**e**) indicate fluorescence radiant efficiency (photons s^{-1} cm^{-2} steradian^{-1} per µW cm^{-2}). Ex., excitation maximum; Em., emission maximum.

Two NIR FPs engineered in this work, iRFP670 and iRFP720, are (to our knowledge) the most blue- and red-shifted BphP-based fluorescent probes reported to date. All five iRFPs have high effective brightness and low cytotoxicity and do not require exogenous BV to fluoresce in mammalian cells or in mice. The multicolor whole-body imaging techniques aided by iRFPs should become common approaches in cell and developmental biology, in studies of cancer and pathogen invasion, and in biomedicine.

METHODS

Methods and any associated references are available in the online version of the paper.

Accession codes. GenBank/EMBL/DDBJ: KC991142 (iRFP670), KC991143 (iRFP682), KC991144 (iRFP702) and KC991145 (iRFP720).

Note: Supplementary information is available in the online version of the paper.

ACKNOWLEDGMENTS

We thank E. Giraud (Institute for Research and Development, France) for the *hmuO* and *Rp*BphP6 genes, F. Subach (currently at the National Research Center "Kurchatov Institute") for the pWA23h plasmid, G. Filonov (currently at Weill Cornell Medical College) for the iRFP713 adenovirus, J. Zhang for assistance in cell sorting, Y. Wang, L.-M. Ting, X. Wang and K. Piatkevich for help with mouse experiments, B. Taylor (PerkinElmer/Caliper) for assistance with the Living Image software and P. Guo for help with the confocal microscope. This work was supported by grants GM073913, CA164468 and EB013571 from the US National Institutes of Health.

AUTHOR CONTRIBUTIONS

D.M.S. developed the proteins and characterized them *in vitro*, in cultured cells and in mice. V.V.V. directed and planned the project. V.V.V. and D.M.S. designed the experiments, analyzed the data and wrote the manuscript.

COMPETING FINANCIAL INTERESTS

The authors declare no competing financial interests.

1. Weissleder, R. *Nat. Biotechnol.* **19**, 316–317 (2001).
2. Strack, R.L. *et al. Biochemistry* **48**, 8279–8281 (2009).
3. Lin, M.Z. *et al. Chem. Biol.* **16**, 1169–1179 (2009).
4. Morozova, K.S. *et al. Biophys. J.* **99**, L13–L15 (2010).
5. Shcherbo, D. *et al. Nat. Methods* **7**, 827–829 (2010).
6. Subach, O.M. *et al. Nat. Methods* **8**, 771–777 (2011).
7. Piatkevich, K.D., Subach, F.V. & Verkhusha, V.V. *Chem. Soc. Rev.* **42**, 3441–3452 (2013).
8. Giraud, E. & Vermeglio, A. *Photosynth. Res.* **97**, 141–153 (2008).
9. Auldridge, M.E. & Forest, K.T. *Crit. Rev. Biochem. Mol. Biol.* **46**, 67–88 (2011).
10. Giraud, E. *et al. J. Biol. Chem.* **280**, 32389–32397 (2005).
11. Shu, X. *et al. Science* **324**, 804–807 (2009).
12. Auldridge, M.E., Satyshur, K.A., Anstrom, D.M. & Forest, K.T. *J. Biol. Chem.* **287**, 7000–7009 (2012).
13. Filonov, G.S. *et al. Nat. Biotechnol.* **29**, 757–761 (2011).
14. Filonov, G.S. *et al. Angew. Chem. Int. Edn. Engl.* **51**, 1448–1451 (2012).
15. Wagner, J.R., Brunzelle, J.S., Forest, K.T. & Vierstra, R.D. *Nature* **438**, 325–331 (2005).
16. Toh, K.C., Stojkovic, E.A., van Stokkum, I.H., Moffat, K. & Kennis, J.T. *Phys. Chem. Chem. Phys.* **13**, 11985–11997 (2011).
17. Strack, R.L. *et al. Nat. Methods* **5**, 955–957 (2008).

ONLINE METHODS

Mutagenesis and screening of libraries. Internal EcoRI sites were removed from genes encoding both *Rp*BphP6 (ref. 8) and iRFP proteins[13] using site-specific mutagenesis. A PCR-amplified BglII-EcoRI fragment encoding *Rp*BphP6 PAS-GAF domains (first 310 amino acids) was cloned into the pBAD/His-B vector (Invitrogen). Site-specific mutagenesis was performed using a QuickChange Mutagenesis Kit (Stratagene). For simultaneous mutagenesis at several positions, an overlap-extension approach was applied[18]. Random mutagenesis was performed using a GeneMorph II Random Mutagenesis Kit (Stratagene) or a Diversity PCR Random Mutagenesis Kit (Clontech) under conditions resulting in a mutation frequency of up to 16 mutations per 1,000 base pairs. After mutagenesis, a mixture of mutated genes was electroporated into LMG194 host cells (Invitrogen) containing the pWA23h plasmid facilitating biliverdin synthesis. The pWA23h plasmid contained the rhamnose promoter from the pWA21 plasmid[19], kanamycin resistance and COLA origin parts from a pCOLADuet-1 plasmid (Novagen). First, the AvrII-PciI fragment containing kanamycin resistance and the COLA origin was PCR amplified from the pCOLADuet-1 plasmid and inserted into a pWA21h-AvrIINotI vector. Then an *hmuO* gene encoding *Bradyrhizobium* ORS278 heme oxygenase[20] was PCR amplified from the pBAD/HisB-*Rp*BphP2-hmuO plasmid[10] and swapped with a gene encoding EGFP in the pWA21-AvrIINotI plasmid.

Typical mutant libraries consisted of about 10^6–10^8 independent clones. The LMG194 cells were grown overnight at 37 °C in RM minimal medium supplemented with ampicillin and kanamycin. Protein expression in the libraries was induced with 0.002% arabinose and 0.02% rhamnose. The cells were grown for 6–8 h at 37 °C and then at 18 °C for 24 h. Before FACS screening, bacterial cells were washed with phosphate-buffered saline (PBS) and diluted with PBS to an optical density of 0.03 at 600 nm. The libraries were screened using MoFlo XDP (Beckman Coulter) fluorescence-activated cell sorter equipped with argon, krypton and argon-krypton mixed-gas lasers. Typically about ten sizes of each library were sorted using a 676-nm laser line for excitation and a 700-nm LP emission filter for positive selection. The brightest collected infrared bacterial cells were rescued in SOC medium at 37 °C for 1 h and then grown on LB/ampicillin/kanamycin Petri dishes supplemented with 0.02% arabinose, 0.2% rhamnose, 100 μM ALA and 50 μM $FeCl_3$ overnight at 37 °C and then incubated at 18 °C. To search for spectrally shifted libraries, we sorted random mutants of iRFP713 and iRFP702 with combinations of two laser lines (647 nm and 676 nm; in some experiments a 592-nm solid-state laser was used instead of 647 nm) and emission filters (670/30 nm and 718 nm LP). The dishes were analyzed with a Leica MZ16F fluorescence stereomicroscope equipped with 650/45-nm excitation and 690-nm LP emission filters (Chroma) and a CCD camera. Screening for spectrally shifted mutants on Petri dishes was performed using the IVIS Spectrum instrument (PerkinElmer/Caliper). Approximately 20–50 clones in each screen were selected. Their spectra, and their brightness in HeLa cells transfected with plasmids—obtained after the FP genes were swapped with a gene encoding EGFP in the pEGFP-N1 plasmid (Clontech)—were tested, and their DNA was sequenced. A mixture of several selected mutants was then used as a template for the next round of mutagenesis.

Protein characterization. The *Rp*BphP6 and iRFP mutants with polyhistidine tags on the N termini were expressed in LMG194 bacterial cells grown in RM medium supplemented with ampicillin, kanamycin, 0.002% arabinose and 0.02% rhamnose for 15–18 h at 37 °C and then for 24 h at 18 °C. Proteins were purified using Ni-NTA agarose (Qiagen) according to the manufacturer's protocol with minor modification. In the wash buffer, 400 mM imidazole was substituted with 100 mM EDTA. Fluorescence spectra were recorded using a FluoroMax-3 spectrofluorometer (Jobin Yvon). A Hitachi U-2000 spectrophotometer was used for absorbance measurements.

The extinction coefficient was calculated from a comparison of absorbance values at the main peak with the absorbance value at the smaller peak at around 390 nm, assuming the latter had an extinction coefficient of free BV of 39,900 M^{-1} cm^{-1}. To determine quantum yield, we compared the fluorescence signal of a purified protein to that of an equally absorbing Nile blue dye. pH titrations were done using a series of buffers (100 mM sodium acetate, 300 mM NaCl for pH 2.5–5.0 and 100 mM NaH_2PO_4, 300 mM NaCl for pH 4.5–9.0).

To study protein folding and maturation in cells[21], we grew LMG194 bacterial cells at 37 °C overnight in RM medium. The next morning, 0.2% rhamnose was added for 2 h, 0.002% arabinose was added, and cells were cultured for 1 h. Then arabinose was washed out, and cells were cultured in RM medium with 0.2% rhamnose at 37 °C. Fluorescence intensities of the equal aliquots of the cell suspension were measured at intervals after dilution to the same optical density of 0.2, and the obtained values were multiplied by the dilution factor. For EGFP expression, the procedure was the same except that the LMG194 strain did not contain the pWA21h plasmid for heme oxygenase expression.

Protein imaging in a phantom mouse. Recombinant far-red GFP-like FPs were expressed in LMG194 bacterial cells and then purified using Ni-NTA agarose (Qiagen). The purified FPs were diluted to equal concentrations of 8 μM, calculated from the extinction coefficients at the chromophore absorbance maxima. A 5-μl volume of each FP was placed 15 mm deep inside into one of two available bores in an XFM-2 phantom mouse (PerkinElmer/Caliper). The bores were located at distances of 7.0 mm and 18.1 mm from the imaging surface. Images were taken in 19 different combinations of the far-red and infrared excitation and emission channels using an epifluorescence mode of the IVIS Spectrum (PerkinElmer/Caliper). A signal-to-background ratio was calculated for each wavelength combination for each FP; the phantom mouse without protein sample inside was used as a background reference. All quantitative measurements of fluorescence signal were performed using the Living Image v.4.3.1 software (PerkinElmer/Caliper). To remove cross-bleed from the excitation light, we performed an adaptive background subtraction.

Mammalian plasmids and cell culture. The plasmids used for expression of all FPs in mammalian cells were based on pEGFP-N1 backbone (Clontech). To construct the plasmids (piRFP670-N1, piRFP682-N1, piRFP702-N1, piRFP713-N1, piRFP720-N1, pmNeptune-N1, pE2-Crimson-N1, peqFP650-N1, peqFP670-N1), we PCR-amplified the respective genes as AgeI-NotI fragments and swapped them with a gene encoding EGFP in pEGFP-N1.

To construct pMito-iRFP670, pMito-iRFP713 and pMito-iRFP720 iRFP670, we cut iRFP713 and iRFP720 genes from N1 plasmids and swapped the with the mTagBFP gene in pMito-mTagBFP[22]. To generate pNLS-iRFP670, pNLS-iRFP713 and pNLS-iRFP720 iRFP670, we cut iRFP713 and iRFP720 genes from the piRFPs-N1 plasmids as AgeI-NotI fragments and swapped them with a gene encoding ECFP in the pNLS-ECFP plasmid.

HeLa cell lines were grown in DMEM containing 10% FBS, 0.5% penicillin-streptomycin and 2 mM glutamine (Invitrogen). For microscopy, cells were cultured in 35-mm glass-bottom culture dishes with no. 1 cover glasses (MatTek). MTLn3 rat adenocarcinoma cells were cultured in αMEM medium (Life Technologies) supplied with 5% FBS, 0.5% penicillin-streptomycin and 2 mM glutamine (Life Technologies). Plasmid transfections were performed using an Effectene reagent (Qiagen) according to the manufacturer's protocol. Stably expressing cells were selected with 700 mg/ml G418 antibiotic. Sorting of positive cells was performed using a MoFlo XDP sorter (Beckman Coulter) equipped with a 676-nm Kr laser and a 700-nm LP emission filter.

Imaging and characterization in mammalian cells. Imaging of HeLa cells was performed 48 h after the transfection. HeLa cells were imaged using an Olympus IX81 inverted epifluorescence microscope equipped with a 200-W Me-Ha arc lamp (Lumen220Pro, standardly equipped with 800-nm cold mirror; Prior), 100×/1.4-NA oil-immersion objective lens (UPlanSApo, Olympus) and far-red (605/40-nm exciter and 640-nm LP emitter) or Cy5.5 filter sets (665/45-nm exciter and 725/50-nm emitter) (Chroma). Two-color imaging of cells cotransfected with iRFP670 and iRFP720 or iRFP670 and iRFP713 was performed with two filter sets (605/40-nm exciter, 667/30-nm emitter and 682/12-nm exciter, 721/42-nm emitter). All filter sets were from Chroma. SlideBook v.4.1 software (Intelligent Imaging Innovations) was used to operate the Olympus IX81 inverted microscope.

Spectral imaging of mixtures of MTLn3 cells stably expressing iRFP670, iRFP682, iRFP702 and iRFP720 was performed using a Leica TCS SP5 confocal microscope (Leica Microsystems). A 63×/1.4-NA oil-immersion objective lens and a 633-nm laser line were used. Emission spectra were detected from 660 nm to 790 nm. The LAS-AF software (Leica Microsystems) was used to operate the microscope and unmix the channels. Spectra of purified FPs were used as references for unmixing. Unmixed channels were pseudocolored and overlaid using ImageJ software (NIH).

Photobleaching experiments were performed in HeLa cells transiently expressing FPs with the Olympus IX81 microscope described above. Raw data were normalized to absorbance spectra and extinction coefficients of the proteins, the spectrum of 200-W Me-Ha arc lamp and the transmission of 665/45-nm photobleaching filter.

For flow cytometry analysis of effective brightness in mammalian HeLa cells, the piRFP-N1 plasmids encoding FPs were cotransfected with pEGFP-N1 to normalize for transfection efficiency. Fluorescence intensity of cells was analyzed using either a LSRII cytometer (BD Biosciences) equipped with 488-nm and 635-nm lasers and using 530/30-nm, 660/20-nm, 710/20-nm and 780/60-nm filters or the similar LSRII cytometer (BD Biosciences) equipped with 488-nm and 640-lasers and using 525/30-nm, 670/30-nm, 730/45-nm and 780/60-nm filters. For cell fluorescence quantification, a mean fluorescence intensity of the non-negative population in the near-infrared channel was divided by a mean fluorescence intensity of the same population in the green channel, thus normalizing the near-infrared signal to the transfection efficiency. All FACS calculations were performed using FlowJo software (Tree Star).

Cytotoxicity was estimated as a stability of fluorescence over cell generations as described before[13]. MTLn3 cells were transfected with plasmids encoding iRFP670, iRFP682, iRFP702, iRFP713, iRFP720 and EGFP. After several days, the drug G418 was added to a final concentration of 700 μg/ml to select for stable preclonal mixtures. On day 14 post-transfection the cells were sorted using the MoFlo XDP cell sorter, and the brightest fluorescent population for each protein was collected. An aliquot of collected cells was analyzed the same day using the LSRII cytometer (10,000 events). After 15 more days of culturing in the presence of G418 (29 d after transfection in total), the cells were analyzed using the LSRII cytometer in the same conditions. Histograms representing cell populations and mean fluorescence intensities of the sorted cells were obtained using FlowJo.

Discrimination of four types of MTLn3 cells stably expressing iRFP670, iRFP682, iRFP702 and iRFP720 (with a single FP type per cell) was performed using the LSRII cytometer with the 635-nm laser and 660/20-nm and 780/60-nm emission filters. Events (10,000) for each cell type were analyzed under the same conditions in one experiment. The obtained dot plots were superimposed.

Construction of adenoviral vectors. The adenovirus serotype V–based particles[23] containing the iRFP were obtained using an AdEasy XL Adenoviral Vector System (Stratagene), as described[13].

***In vivo* imaging.** To implant xenograph tumors, 10^6 MTLn3 cells stably expressing iRFP670, iRFP682, iRFP702, iRFP713, iRFP720 or EGFP (with a single FP type per cell) were injected into the mammary gland of SCID/NCr mice (female, 5–7 weeks old) (Taconic) and imaged starting 1 week later using the IVIS Spectrum in epifluorescence mode. All mice were imaged in 19 filter channels using the IVIS Spectrum. Belly fur was removed using a depilatory cream. Mice were fed with AIN-93M Maintenance Purified Diet (TestDiet) to reduce the intrinsic autofluorescence level. All quantitative measurements of fluorescence signal were made with Living Image.

For fluorescence time-course measurement, mice with a single tumor were imaged over 4 weeks after cell injection. Background-subtracted images of total radiant efficiencies of the same region over tumors were generated. Filter channels used for calculation of tumor growth curves were the following: 640/30-nm exciter and 680/20-nm emitter for iRFP670; 675/30-nm exciter and 720/20-nm emitter for iRFP682, iRFP702, iRFP713; and 710/30-nm exciter and 710/760-nm emitter for iRFP720.

For two-color imaging of two tumors, mice were injected with MTLn3 cells expressing either iRFP670 or iRFP720 in close sites the same day or with a time difference of 1 week. For two-color imaging of iRFP670-expressing tumor and iRFP713-expressing liver, mice with a xenograph tumor expressing iRFP670 were intravenously injected with 2×10^9 infectious units of an adenovirus at day 18 or 24 after MTLn3 cell injection.

doi:10.1038/nmeth.2521

For spectral imaging of five FPs, mice were injected with two types of MTLn3 cells each on the same day. For spectral unmixing, an image cube was collected on the IVIS Spectrum with 19 filter channels. Fluorescence regions were identified and spectrally unmixed using Living Image. Spectral data obtained for individual bacterial streaks expressing iRFP670, iRFP682, iRFP702, iRFP713 or iRFP720 were used as references for unmixing.

For fluorescence imaging tomography (FLIT), mice were depilated, and images were taken in transillumination mode. Data acquisition and processing were performed according to the Living Image v.4.3.1 protocol. Two fluorescence samples were imaged with different filter sets (640/30-nm exciter and 680/20-nm emitter for iRFP670, 710/30-nm exciter and 710/60-nm emitter for iRFP713) and then overlaid.

The tumors and livers were excised postmortem and imaged using the IVIS Spectrum. All animal experiments were performed in an AAALAC approved facility using protocols approved by the Albert Einstein College of Medicine Animal Usage Committee.

18. Ho, S.N., Hunt, H.D., Horton, R.M., Pullen, J.K. & Pease, L.R. *Gene* **77**, 51–59 (1989).
19. Wegerer, A., Sun, T. & Altenbuchner, J. *BMC Biotechnol.* **8**, 2 (2008).
20. Giraud, E. *et al. Photochem. Photobiol. Sci.* **3**, 587–591 (2004).
21. Kremers, G.J., Goedhart, J., van den Heuvel, D.J., Gerritsen, H.C. & Gadella, T.W. Jr. *Biochemistry* **46**, 3775–3783 (2007).
22. Subach, O.M. *et al. Chem. Biol.* **15**, 1116–1124 (2008).
23. Waddington, S.N. *et al. Cell* **132**, 397–409 (2008).

Near-infrared fluorescent proteins for multicolor *in vivo* imaging

Daria M. Shcherbakova & Vladislav V. Verkhusha

Supplementary Figure 1	Alignment of the amino acid sequences of iRFPs with their *Rp*BphP2 and *Rp*BphP6 templates.
Supplementary Figure 2	Biochemical properties of iRFPs.
Supplementary Figure 3	Intracellular distribution of fluorescence and intracellular photostability of BphP-based FPs in live cells.
Supplementary Figure 4	Comparison of iRFP670 with GFP-like far-red FPs in flow cytometry.
Supplementary Figure 5	Characterization of iRFPs as probes for *in vivo* imaging experiments.
Supplementary Figure 6	Growth of tumors expressing iRFPs in mice.
Supplementary Figure 7	Two-color imaging of cells and tumors expressing iRFPs using two standard filter channels.
Supplementary Figure 8	Noninvasive fluorescence imaging tomography of tumor expressing iRFP670 and liver expressing iRFP713 in a mouse.
Supplementary Figure 9	Two-color imaging of tumor and liver isolated from a mouse injected with MTLn3 cells expressing iRFP670 and infected with adenovirus encoding iRFP713.
Supplementary Figure 10	Two-color microscopy of subcellular structures in cells co-expressing two iRFPs.
Supplementary Figure 11	Flow cytometry analysis of MTLn3 cells stably expressing iRFP670, iRFP682, iRFP702 and iRFP720.
Supplementary Figure 12	Multicolor spectral imaging of bacterial streaks expressing iRFPs.
Supplementary Figure 13	Multicolor spectral imaging of isolated tumors expressing iRFPs.

Nature Methods: doi:10.1038/nmeth.2521

Supplementary Figure 1. Alignment of the amino acid sequences of iRFPs with *Rp*BphP2 and *Rp*BphP6 templates.

```
           1        10        20        30        40          50        60
RpBphP2    MTEGSVARQPDLSTCDDEPIHIPGAIQPHGLLLALAADMTIV-AGSDNLPELTGLAIGALIGRSA
iRFP713    MAEGSVARQPDLLTCDDEPIHIPGAIQPHGLLLALAADMTIV-AGSDNLPELTGLAIGALIGRSA
iRFP682    MAEGSVARQPDLLTCDDEPIHIPGAIQPHGLLLALAADMTIV-AGSDNLPELTGLAIGALIGRSA
iRFP720    MAEGSVARQPDLLTCDDEPIHIPGAIQPHGLLLALAADMTIV-AGSDNLPELTGLAIGALIGRSA
RpBphP6    MPRK-----VDLTSCDREPIHIPGSIQPCGCLLACDAQAVRITRISENAGAFFGRETPRVGELLA
iRFP702    MARK-----VDLTSCDREPIHIPGSIQPCGCLLACDAQAVRITRITENAGAFFGRETPRVGELLA
iRFP670    MARK-----VDLTSCDREPIHIPGSIQPCGCLLACDAQAVRITRITENAGAFFGRETPRVGELLA

                70        80        90        100       110       120
RpBphP2    ADVFDSETHNRLTIALAEPGAAVGAPIAVGFTMRKDAGFVGSWHRHDQLVFLELEPPQRDVAEPQ
iRFP713    ADVFDSETHNRLTIALAEPGAAVGAPITVGFTMRKDAGFIGSWHRHDQLIFLELEPPQRDVAEPQ
iRFP682    ADVFDSETHNRLTIALAEPGAAVGAPITVGFTMRKDAGFIGSWHRHDQLIFLELEPPQRDVAEPQ
iRFP720    ADVFDSETHNRLTIALAEPGAAVGAPITVGFTMRKDAGFIGSWHRHDQLIFLELEPPQRDVAEPQ
RpBphP6    DYFGETEAHALRNALAQSSDPKRPALIFGWRDGLTGRTFDISLHRHDGTSIVEFEPAAADQADNP
iRFP702    DYFGETEAHALRNALAQSSDPKRPALIFGWRDGLTGRTFDISLHRHDGTSIVEFEPAAAEQADNP
iRFP670    DYFGETEAHALRNALAQSSDPKRPALIFGWRDGLTGRTFDISLHRHDGTSIIEFEPAAAEQADNP

           130       140       150       160       170       180       190
RpBphP2    AFFRRTNSAIRRLQAAETLESACAAAAQEVREITGFDRVMIYRFASDFSGEVIAEDRCAEVESYL
iRFP713    AFFRRTNSAIRRLQAAETLESACAAAAQEVRKITGFDRVMIYRFASDFSGEVIAEDRCAEVESKL
iRFP682    AFFRRTNSAIRRLQAAETLESACAAAAQEVRKITGFDRVMIYRFASDFSGVVIAEDRCAEVESKL
iRFP720    AFFRRTNSAIRRLQAAETLESACAAAAQEVRKITGFDRVMIYRFASDFSGSVIAEDRCAEVESKL
RpBphP6    L--RLTRQIIARTKELKSLEEMAARVPRYLQAMLGYHRVMMYRFADDGSGKVIGEAKRSDLESFL
iRFP702    L--RLTRQIIARTKELKSLEEMAARVPRYLQAMLGYHRVMLYRFADDGSGKVIGEAKRSDLESFL
iRFP670    L--RLTRQIIARTKELKSLEEMAARVPRYLQAMLGYHRVMLYRFADDGSGMVIGEAKRSDLESFL

                200       210       220       230       240       250
RpBphP2    GLHFPASDIPAQARRLYTINPVRIIPDINYRPVPVTPDLNPVTGRPIDLSFAILRSVSPVHLEYM
iRFP713    GLHYPASTVPAQARRLYTINPVRIIPDINYRPVPVTPDLNPVTGRPIDLSFAILRSVSPVHLEFM
iRFP682    GLHYPASAVPAQARRLYTINPVRIIPDINYRPVPVTPDLNPVTGRPIDLSFAILRSVSPCHLEFM
iRFP720    GLHYPASFIPAQARRLYTINPVRIIPDINYRPVPVTPDLNPVTGRPIDLSFAILRSVSPNHLEFM
RpBphP6    GQHFPASDIPQQARLLYLKNAIRVISDSRGISSRIVPERDAS-GAALDLSFAHLRSVSPIHLEYL
iRFP702    GQHFPASLVPQQARLLYLKNAIRVVSDSRGISSRIVPEHDAS-GAALDLSFAHLRSISPIHLEFL
iRFP670    GQHFPASLVPQQARLLYLKNAIRVVSDSRGISSRIVPEHDAS-GAALDLSFAHLRSISPCHLEFL

           260       270       280       290       300       310
RpBphP2    RNIGMHGTMSISILRGERLWGLIACHHRKPNYVDLDGRQACELVAQVLAWQIGVMEE
iRFP713    RNIGMHGTMSISILRGERLWGLIVCHHRTPYYVDLDGRQACELVAQVLAWQIGVMEE
iRFP682    RNIGMHGTMSISILRGERLWGLIVCHHRTPYYVDLDGRQACELVAQVLAWQIGVMEE
iRFP720    RNIGMHGTMSISILRGERLWGLIVCHHRTPYYVDLDGRQACELVAQVLAWQIGVMEE
RpBphP6    RNMGVSASMSLSIIIDGTLWGLIACHHYEPRAVPMAQRVAAEMFADFFSLHFTAAHHQR
iRFP702    RNMGVSASMSLSIIIDGTLWGLIICHHYEPRAVPMAQRVAAEMFADFLSLHFTAAHHQR
iRFP670    RNMGVSASMSLSIIIDGTLWGLIICHHYEPRAVPMAQRVAAEMFADFLSLHFTAAHHQR
```

Mutations introduced into iRFPs comparing to *Rp*BphP2 and *Rp*BphP6 are highlighted in green and in yellow, respectively. The numbering of amino acid residues follows that for *Rp*BphP2. An alanine residue in the second position in iRFPs (highlighted in blue) was introduced to optimize the Kozak sequence for expression in mammalian cells.

Nature Methods: doi:10.1038/nmeth.2521

Supplementary Figure 2. Biochemical properties of iRFPs.

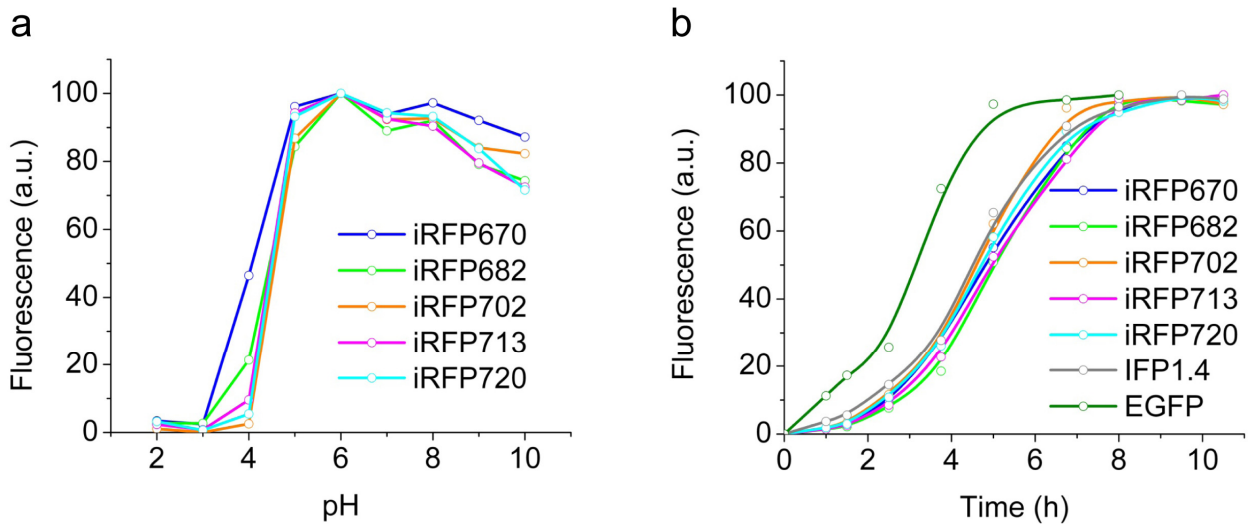

(**a**) pH dependence of fluorescence. (**b**) Folding and chromophore formation kinetics of BphP-based FPs and conventional EGFP in bacteria. Time "0" corresponds to the beginning of the 1 h long pulse-chase induction of the protein expression.

Nature Methods: doi:10.1038/nmeth.2521

Supplementary Figure 3. Intracellular distribution of fluorescence and intracellular photostability of BphP-based FPs in live cells.

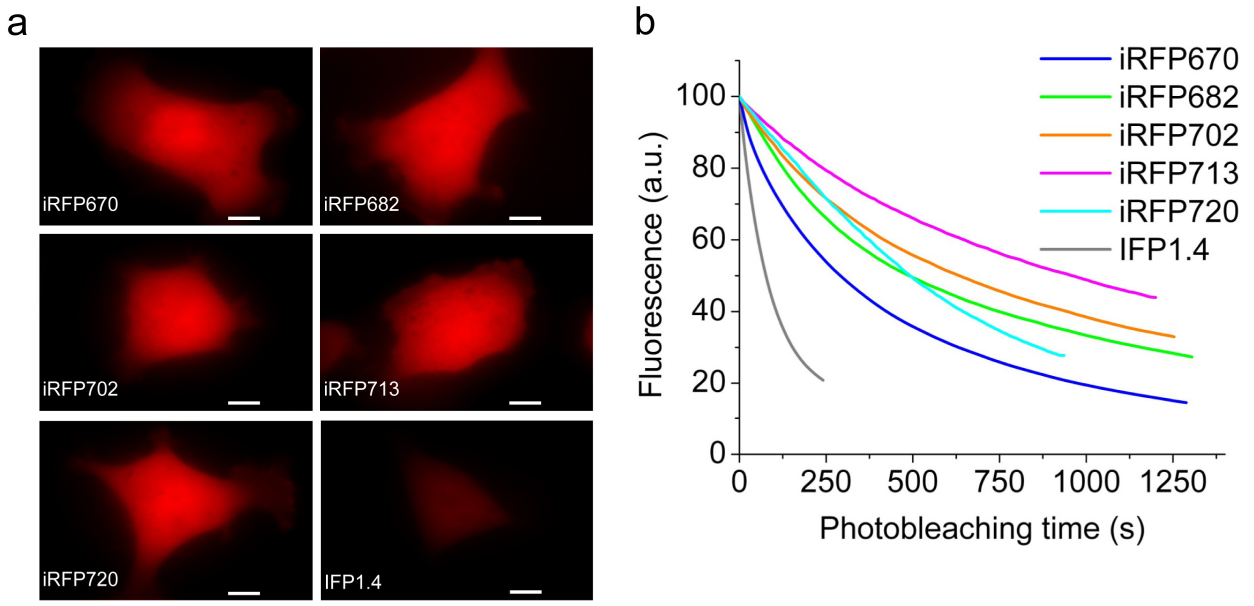

(**a**) Fluorescent images of the transiently transfected Hela cells. iRFP670 was imaged with an excitation filter 605/40 nm and an emission filter 640 nm LP, all other FPs – with an excitation filter 665/45 nm and an emission filter 725/50 nm. Scale bar is 10 μm. (**b**) Photobleaching in HeLa cells. The curves were normalized to absorbance spectra and extinction coefficients of FPs, spectrum of the lamp and transmission of an excitation filter.

Nature Methods: doi:10.1038/nmeth.2521

Supplementary Figure 4. Comparison of iRFP670 with GFP-like far-red FPs in flow cytometry.

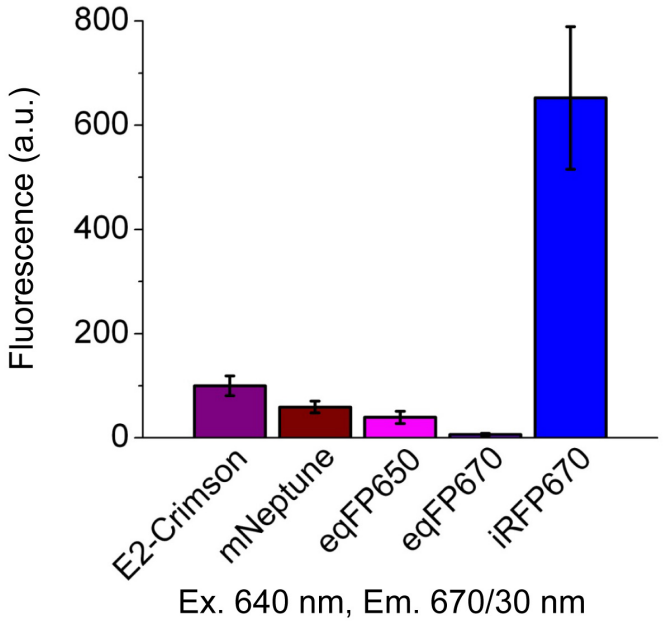

Mean fluorescence intensities of transiently transfected HeLa cells expressing FPs excited with 640 nm laser in flow cytometry. Positive populations of cells were analyzed. The values were normalized to transfection efficiency using co-transfected EGFP. The signal of E2-Crimson, the brightest GFP-like far-red FP in this experiment, was normalized to 100%. Error bars, s.d. (n = 3 transfection experiments).

Nature Methods: doi:10.1038/nmeth.2521

Supplementary Figure 5. Characterization of iRFPs as probes for *in vivo* imaging experiments.

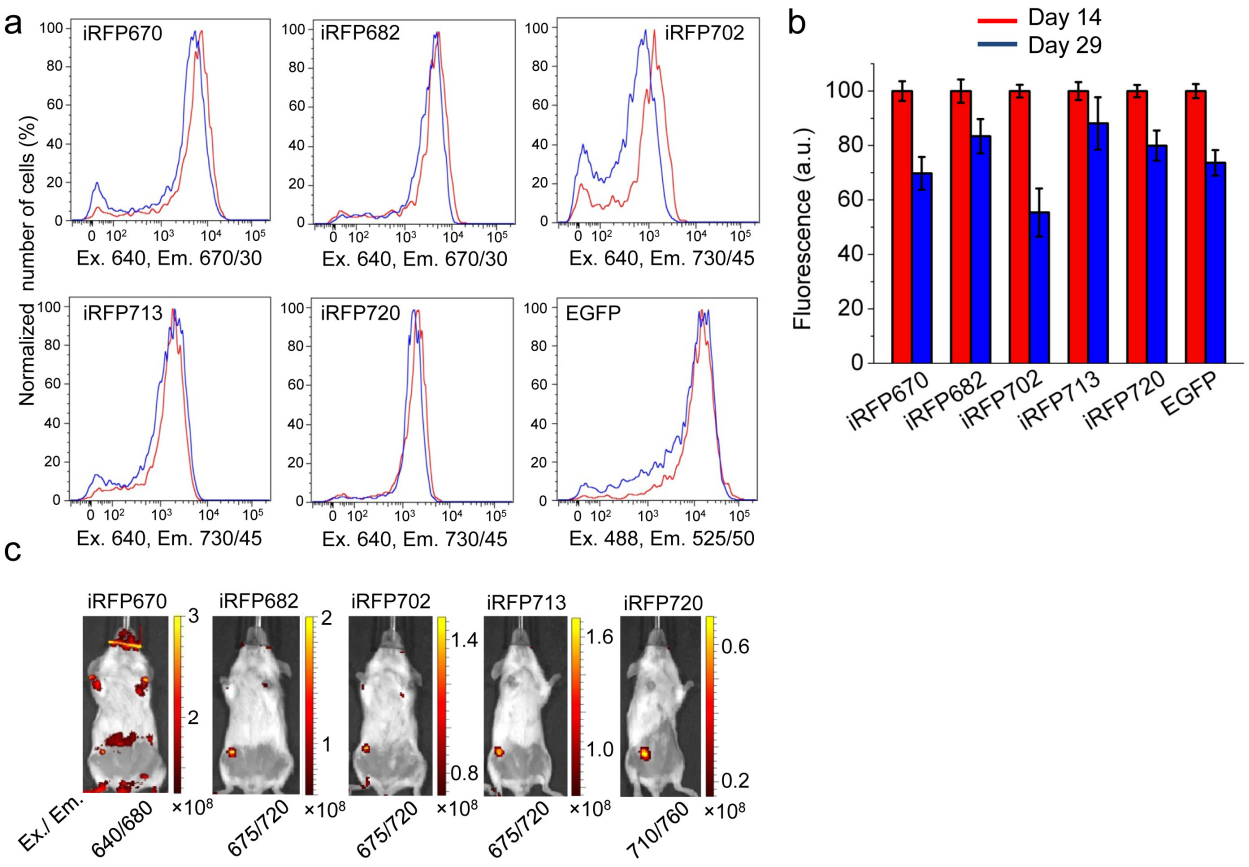

(**a,b**) Cytotoxicity of iRFPs compared to EGFP estimated as a stability of fluorescence over cell generations in prolonged expression conditions. (a) 10,000 MTLn3 cells stably expressing FPs were analyzed by flow cytometry on day 14 (in red) and on day 29 (in blue) after transfection. Representative populations are shown. Number of cells (counts) was normalized to the maximum values for each plot. Emission filters and lasers used for analysis are indicated. (b) Quantification of the mean fluorescence intensities of MTLn3 cells in the experiment described in (a). The values were normalized to the initial signal on day 14 for each FP. Error bars, s.d. (*n* = 3). (**c**) Early detection of tumors expressing iRFPs in living mice. Representative images of mice on day 8 after the cell injection. Excitation and emission maxima of filter channels are indicated. The color bar displays the fluorescent radiant efficiency ([photon/s/cm^2/steradian]/[μW/cm^2]).

Nature Methods: doi:10.1038/nmeth.2521

Supplementary Figure 6. Growth of tumors expressing iRFPs in mice.

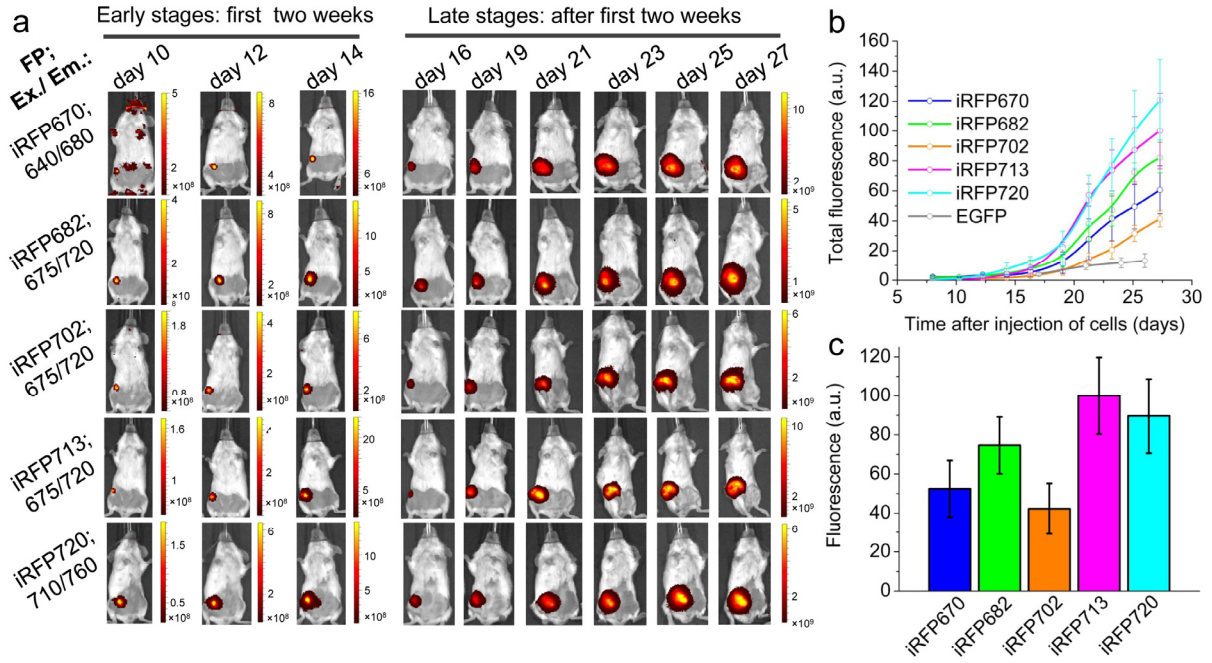

(**a**) Xenograph tumors implanted by injection of stably expressing rat adenocarcinoma MTLn3 cells in immunocompromized mice. Representative images of mice at early and late stages of tumor growth are shown. Expressed FP, excitation and emission maxima of filter channels are indicated on the left. The color bars indicate the fluorescent radiant efficiency ([photon/s/cm^2/steradian]/[μW/cm^2]). (**b**) Total fluorescence of tumors expressing iRFPs had been imaged for 4 weeks. Total fluorescence efficiencies were normalized to the maximum value for iRFP713-expressing tumors, excitation efficiency of each FP with light passed through excitation filter fluorescence signal of each FP in the emission filter. Error bars, s.d. (n = 3). (**c**) Brightness of MTLn3 cells stably expressing iRFPs used for implantation of xenograft tumors. Brightness of preclonal mixtures of MTLn3 cells stably expressing iRFPs. Mean fluorescence intensities were normalized to excitation efficiency of each FP with the 640 nm laser, and fluorescence signal of each FP in the emission filter. Fluorescence signal of iRFP713 was normalized to 100%. Error bars, s.d. (n = 3).

Nature Methods: doi:10.1038/nmeth.2521

Supplementary Figure 7. Two-color imaging of cells and tumors expressing iRFPs using two standard filter channels.

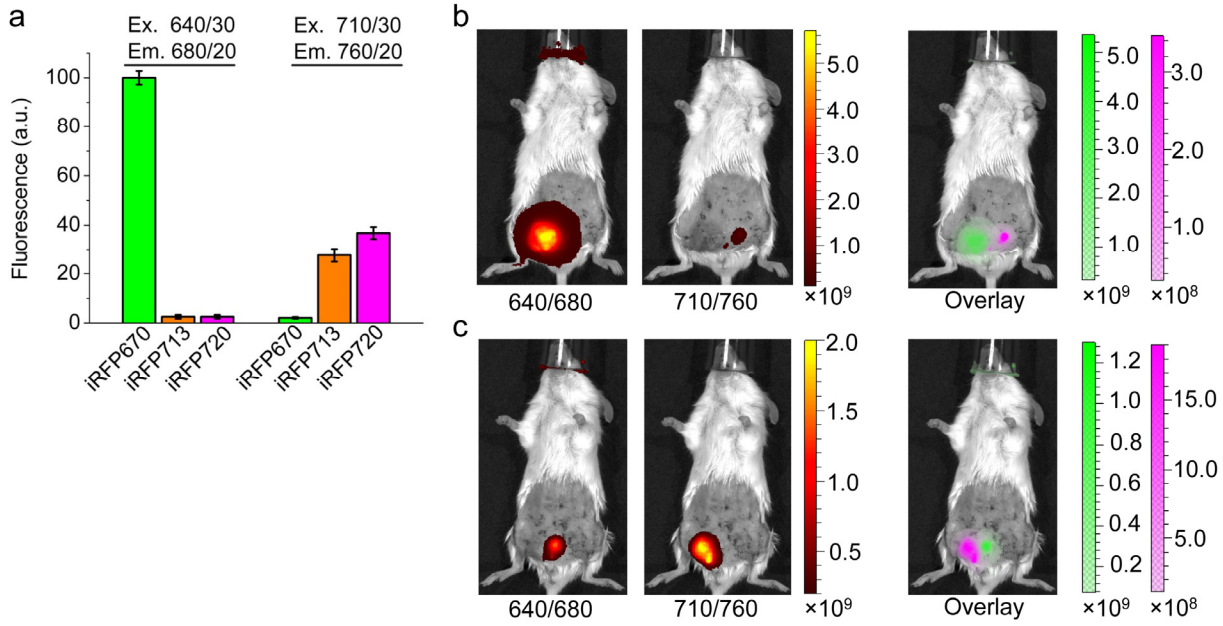

(a) Fluorescence signals of iRFP670, iRFP713, and iRFP720 imaged using the two standard filter channels available on IVIS Spectrum instrument (excitation/emission maxima at 640 nm/680 nm and 710 nm/760 nm). Average radiant efficiencies were measured in bacterial streaks expressing each FP. The values were normalized to the maximal signal for iRFP670. Error bars, s.d. (n = 3). (**b,c**) Images of living mice with tumors expressing iRFP670 (left tumor) and iRFP720 (right tumor). Mice were injected with MTLn3 cells expressing either (b) iRFP670 or (c) iRFP720 first, then on day 8 they were injected again with MTLn3 cells of another type, expressing iRFP720 (b) or iRFP670 (c). Representative images of mice in two optimal channels and the overlays were obtained on day 14 after the second injection. The color bars indicate the fluorescent radiant efficiency ([photon/s/cm^2/steradian]/[μW/cm^2]).

Nature Methods: doi:10.1038/nmeth.2521

Supplementary Figure 8. Noninvasive fluorescence imaging tomography of tumor expressing iRFP670 and liver expressing iRFP713 in a mouse.

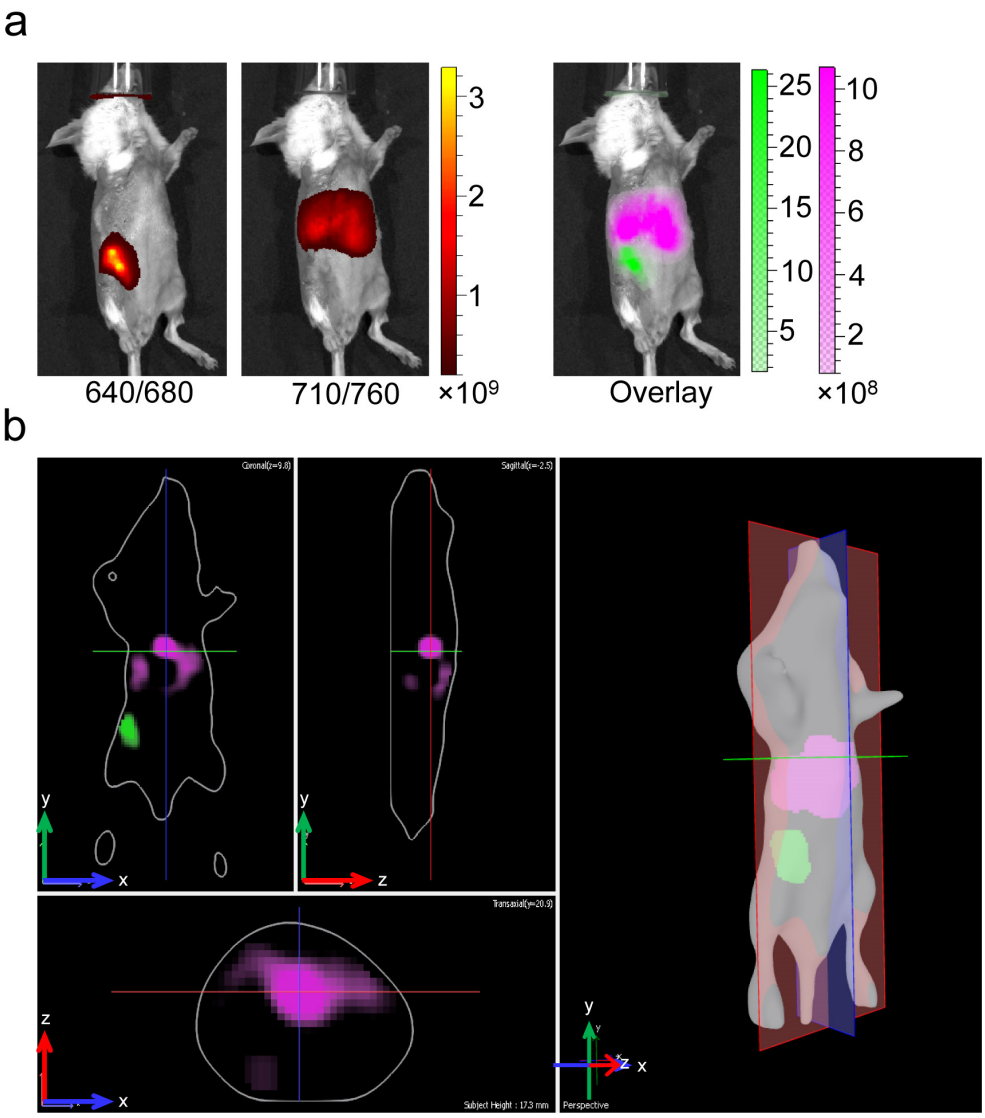

(**a**) Mouse with a xenograft tumor expressing iRFP670 was infected with liver-specific adenovirus encoding iRFP713. Representative epifluorescent images of a mouse on day 18 after cell injection and day 7 after adenovirus infection in two optimal channels and the overlay are shown. The color bar indicates the fluorescent radiant efficiency ([photon/s/cm^2/steradian]/[μW/cm^2]). (**b**) Fluorescent imaging tomography of the mouse shown in (a). Coronal, sagittal, and transaxial sections are shown on the left, and composite side view is shown on the right. Blue, green, and red arrows indicate left-right, rostral-caudal, and dorsoventral axes, respectively.

Nature Methods: doi:10.1038/nmeth.2521

Supplementary Figure 9. Two-color imaging of tumor and liver isolated from a mouse injected with MTLn3 cells expressing iRFP670 and infected with adenovirus encoding iRFP713.

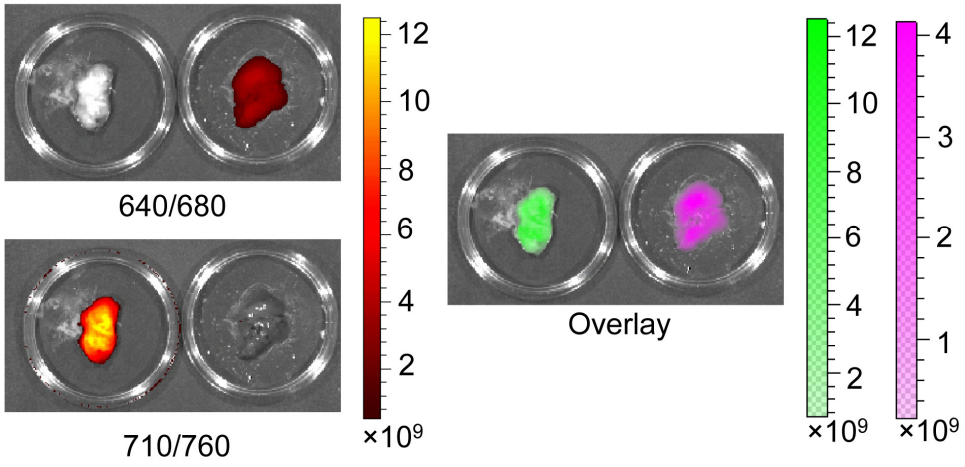

A mouse with a xenograft tumor expressing iRFP670 was infected with adenovirus encoding iRFP713. Representative images of tumor (left) and liver (right) isolated from a mouse on day 29 after cell injection and day 6 after adenovirus infection in two optimal channels and the overlay. The color bar indicates the fluorescent radiant efficiency ([photon/s/cm^2/steradian]/[μW/cm^2]).

Nature Methods: doi:10.1038/nmeth.2521

Supplementary Figure 10. Two-color microscopy of subcellular structures in cells co-expressing two iRFPs.

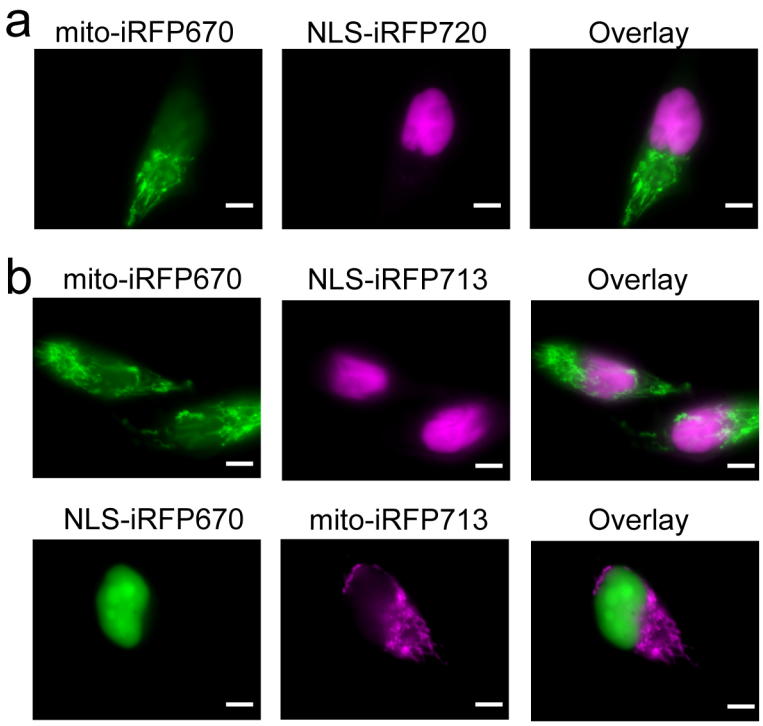

(**a,b**) Images of representative transiently transfected HeLa cells co-expressing iRFP670 and iRFP720 (a), or iRFP670 and iRFP713 (b) in nucleus and mitochondria. iRFP670 was imaged using 605/40 nm excitation and 667/30 nm emission filters (left column, green pseudocolor). iRFP720 and iRFP713 was imaged using 682/12 nm excitation and 721/42 nm emission filters (middle column, magenta pseudocolor). The right column is the overlay of two pseudocolor images. Scale bar, 10 μm.

Nature Methods: doi:10.1038/nmeth.2521

Supplementary Figure 11. Flow cytometry analysis of MTLn3 cells stably expressing iRFP670, iRFP682, iRFP702 and iRFP720.

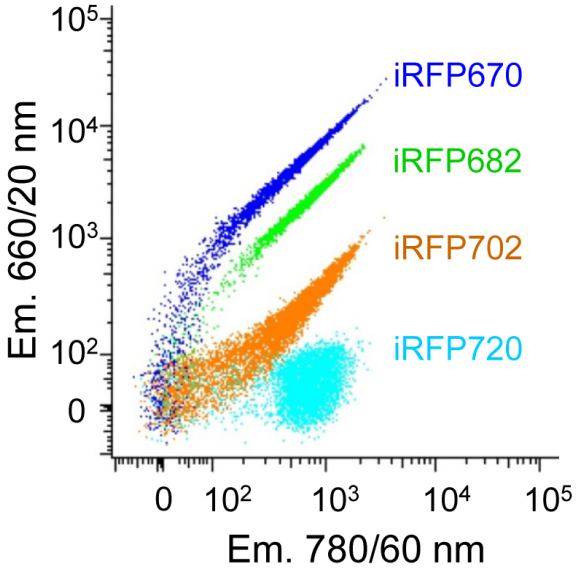

A 635 nm excitation laser and a combination of two indicated emission filters were used. 10,000 events were analyzed for each cell type.

Nature Methods: doi:10.1038/nmeth.2521

Supplementary Figure 12. Multicolor spectral imaging of bacterial streaks expressing iRFPs**.**

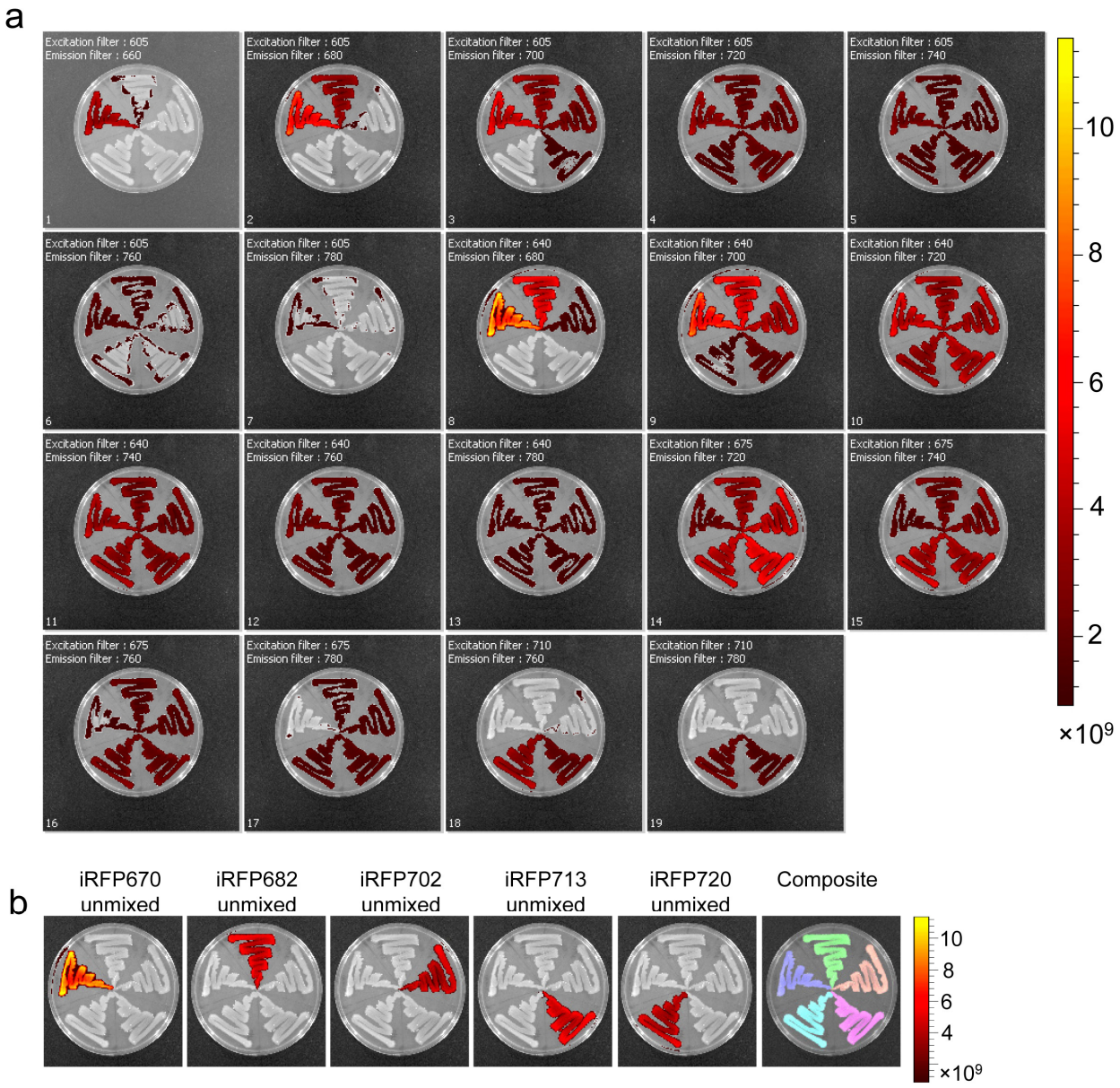

(**a**) Images of a dish with 5 bacterial streaks expressing different iRFPs in 19 spectral channels obtained using IVIS Spectrum. FPs are expressed in the following order, from upper left clockwise: iRFP670, iRFP682, iRFP702, iRFP713, and iRFP720. (**b**) Spectrally unmixed signals and a composite pseudocolored image are shown. Spectra corresponding to individual bacterial streaks were used as references for unmixing procedure. The color bar indicates the fluorescent radiant efficiency ([photon/s/cm^2/steradian]/[μW/cm^2]).

Nature Methods: doi:10.1038/nmeth.2521

Supplementary Figure 13. Multicolor spectral imaging of isolated tumors expressing iRFPs.

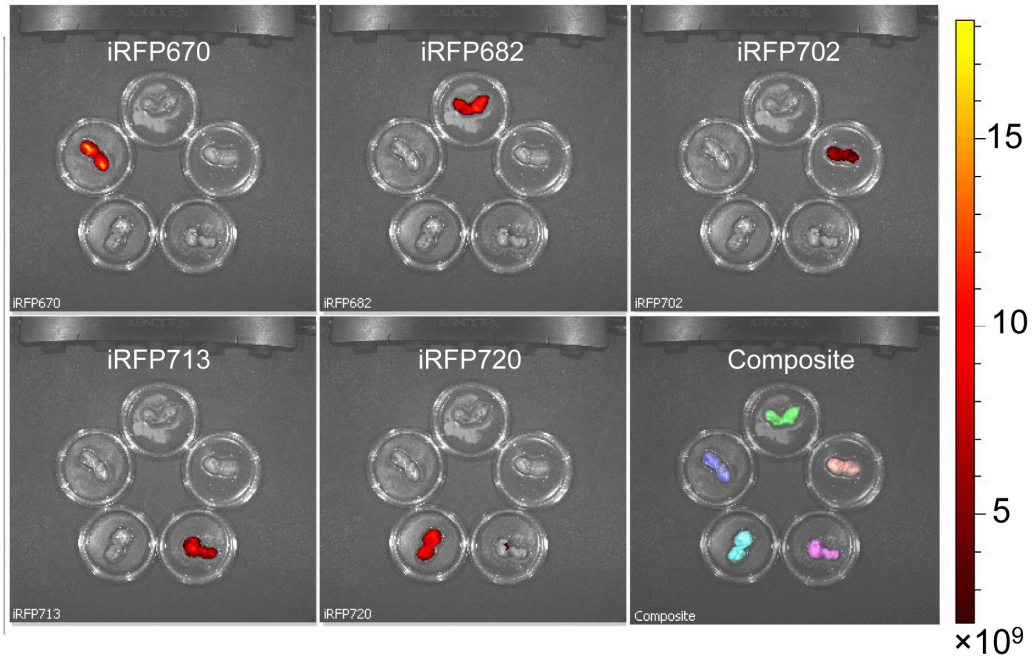

Mice were injected with MTLn3 cells stably expressing 5 iRFPs. Tumors were isolated on day 28 after the cell injection. 19 spectral channels were acquired on IVIS Spectrum and spectrally unmixed using reference spectra of iRFPs. Spectrally unmixed channels and composite pseudocolored image are shown. The tumors express iRFPs in the following order, from upper left clockwise: iRFP670, iRFP682, iRFP702, iRFP713, and iRFP720. The color bar indicates the fluorescent radiant efficiency ([photon/s/cm^2/steradian]/[μW/cm^2]).

Nature Methods: doi:10.1038/nmeth.2521